Quantifying measurement fluctuations from stochastic surface processes on sensors with heterogeneous sensitivity - Supplemental Material

Jérôme Charmet*[1], Thomas C. T. Michaels*[1], Ronan Daly[2], Abhinav Prasad[3], Pradyumna Thiruvenkathanathan[3], Robin S. Langley[4], Tuomas P. J. Knowles[1], and Ashwin A. Seshia[3]
[1]*Department of Chemistry, University of Cambridge, Lensfield Road, Cambridge CB2 1EW, United Kingdom*
[2]*Institute for Manufacturing, Engineering Department, University of Cambridge, Charles Babbage Road, Cambridge, CB3 0FS, UK*
[3]*Nanoscience Centre, Engineering Department, University of Cambridge, 11 J.J. Thomson Avenue, Cambridge, CB3 0FF, UK and*
[4]*Engineering Department, University of Cambridge, Trumpington Street, Cambridge, CB2 1PZ, UK*
(Dated: June 7, 2016)

EXPERIMENTAL DETAILS

The resonators used for the experiments were fabricated by MEMSCAP, a commercial foundry. They have a thickness of 10 µm and lateral dimensions of 825 µm. The measurements took place in a *Lakeshore* probe station, under vacuum (below 2×10^{-4} mbar) at 300° K. A two port measurement set-up was used to study the resonator in an open loop using an *Agilent 4936B* network analyzer. The measurements were performed using resonators electrostatically excited in the Lameé mode using a bias voltage $V_{dc} = 40$ V and a harmonic AC excitation power of 0 dBm. The frequency and Q factors are extracted from the measured admittance after capacitive feed-through cancellation (V_{dc}= 0 V) using a Lorentzian fit. After the base vacuum has been reached and the temperature stabilised (approx. 3 hours), the frequency stability is below 0.1 ppm (measured over 12 hours, data not shown). Polystyrene (PS) micro-particles (diameter 10 µm, standard deviation < 0.2 µm) from Fluka are positioned on the resonator using a tungsten probe of 10 µm radius. The data presented in Figure 1 comes from a set of measurements presented in Figure (S.1) that shows the frequency shift induced by four PS particles placed on different locations on the sensor. The parts in grey show the resonance frequency ($\Delta f = 0$ Hz) recorded before and after measuring the frequency shifts induced by the particles. The set of measurements took less than 1 hour and the shift recorded after the particles were removed is below 2 Hz compared to the initial measurement. Even though it is slightly higher than 0.1 ppm stability (which would give 0.5 Hz/hour max.), it indicates that the measurement procedure only induces small variations attributed to contamination transferred from the particles to the resonator during the measurement. An image of the resonators and the particles was recorded for each measurement. The images were processed and the coordinates of the PS particles were extracted using *ImageJ 1.45s*. Identical measurements were repeated on a number of occasions to confirm the results (data not shown).

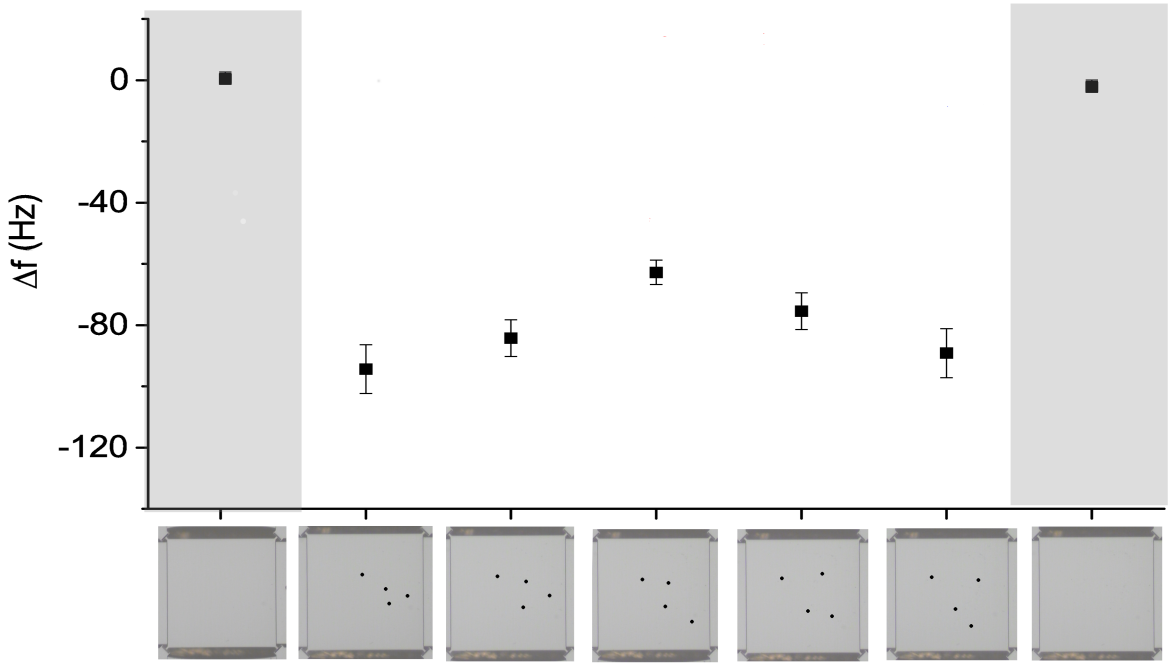

FIG. 1: Frequency shifts induced by 4 PS particles placed on different location on the sensor. The grey areas indicate measurements without particles on the resonator, left and right areas represent measurements before the particles were placed on the resonator and after they were removed respectively. The images have been post-processed to show the position of the particles more clearly.

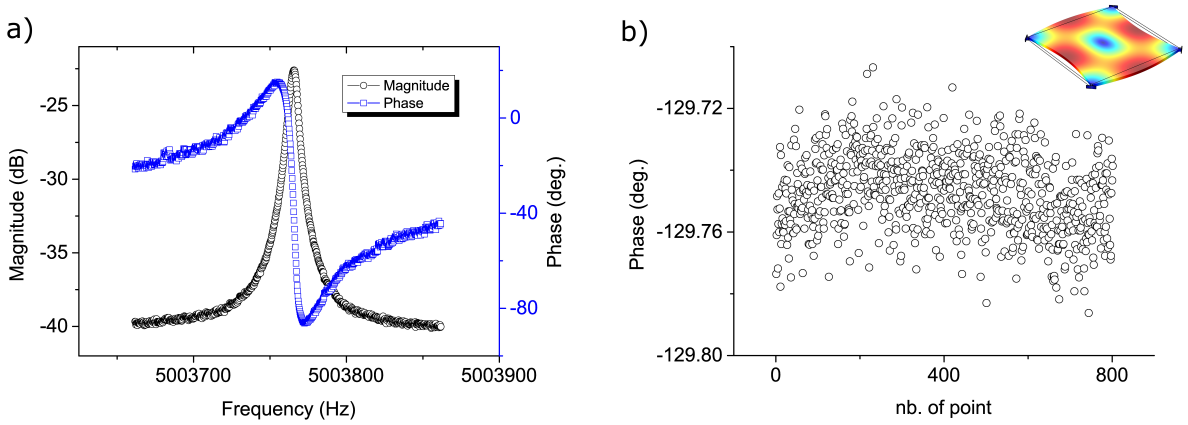

FIG. 2: Characterisation of the resonator excited in the Lamé mode. a) Magnitude and phase at resonance, b) zero span phase noise. Bias voltage $V_{dc} = 60$V

RELATIVE VARIANCE - CLOSED FORM EXPRESSION

Detailed derivation of $\mathbb{E}[(\Delta\tilde{m})]$

Let $g(n)$ be the distribution of the number of objects (i.e. the probability that the number of object equals n). Then, we have

$$\mathbb{E}[(\Delta\tilde{m})] = \mathbb{E}\left[\sum_{j=1}^{N} m_j\varphi^2(\boldsymbol{x}_j)\right] \tag{1}$$

$$= \sum_{n=0}^{\infty} \mathbb{E}\left[\sum_{j=1}^{N} m_j\varphi^2(\boldsymbol{x}_j)\middle| N=n\right] \tag{2}$$

$$= \sum_{n=0}^{\infty} Prob(N=n)\mathbb{E}\left[\sum_{j=1}^{n} m_j\varphi^2(\boldsymbol{x}_j)\right] \tag{3}$$

$$= \sum_{n=0}^{\infty} g(n)\mathbb{E}\left[\sum_{j=1}^{n} m_j\varphi^2(\boldsymbol{x}_j)\right]. \tag{4}$$

Now, we use the linearity of the expectation

$$\mathbb{E}[(\Delta\tilde{m})] = \sum_{n=0}^{\infty} g(n)\mathbb{E}\left[\sum_{j=1}^{n} m_j\varphi^2(\boldsymbol{x}_j)\right] \tag{5}$$

$$= \sum_{n=0}^{\infty} g(n)\sum_{j=1}^{n} \mathbb{E}[m_j\varphi^2(\boldsymbol{x}_j)] \tag{6}$$

$$= \sum_{n=0}^{\infty} g(n)n\cdot\langle m\rangle\mathbb{E}[\varphi^2(\boldsymbol{x}_j)] \tag{7}$$

$$= \frac{\langle N\rangle\langle m\rangle}{M} \tag{8}$$

Detailed derivation of $\mathbb{E}[(\Delta\tilde{m})^2]$

Let $g(n)$ be the distribution of the number of objects (i.e. the probability that the number of object equals n). Then, we have

$$\mathbb{E}[(\Delta\tilde{m})^2] = \mathbb{E}\left[\left(\sum_{j=1}^{N} m_j\varphi^2(\boldsymbol{x}_j)\right)^2\right] \tag{9}$$

$$= \sum_{n=0}^{\infty} \mathbb{E}\left[\left(\sum_{j=1}^{N} m_j\varphi^2(\boldsymbol{x}_j)\right)^2\middle| N=n\right] \tag{10}$$

$$= \sum_{n=0}^{\infty} Prob(N=n)\mathbb{E}\left[\left(\sum_{j=1}^{n} m_j\varphi^2(\boldsymbol{x}_j)\right)^2\right] \tag{11}$$

$$= \sum_{n=0}^{\infty} g(n)\mathbb{E}\left[\left(\sum_{j=1}^{n} m_j\varphi^2(\boldsymbol{x}_j)\right)^2\right]. \tag{12}$$

Now, we can simplify the double sum as usual because n is fixed (no longer a random variable):

$$\sum_{i=1}^{n}\sum_{j=1}^{n} m_i m_j \varphi^2(\boldsymbol{x}_i)\varphi^2(\boldsymbol{x}_j) \tag{13}$$

$$= \sum_{i=1}^{n} m_i^2 \varphi^4(\boldsymbol{x}_i) + \sum_{i=1}^{n}\sum_{j\neq i} m_i m_j \varphi^2(\boldsymbol{x}_i)\varphi^2(\boldsymbol{x}_j).$$

Hence, we obtain

$$\mathbb{E}[(\Delta\tilde{m})^2] = \sum_{n=0}^{\infty} g(n)\mathbb{E}\left[\left(\sum_{j=1}^{n} m_j \varphi^2(\boldsymbol{x}_j)\right)^2\right] \tag{14}$$

$$= \sum_{n=0}^{\infty} g(n) n \cdot \langle m^2\rangle \mathbb{E}[\varphi^4(\boldsymbol{x}_j)] + \tag{15}$$

$$\sum_{n=0}^{\infty} g(n) n(n-1) \cdot \langle m\rangle^2 \mathbb{E}[\varphi^2(\boldsymbol{x}_j)]^2 \tag{16}$$

$$= \langle N\rangle\langle m^2\rangle\mathbb{E}[\varphi^4(\boldsymbol{x}_i)] + \frac{\langle N(N-1)\rangle\langle m\rangle^2}{M^2}. \tag{17}$$

TRANSPORT AND REACTION

This section shows that the sensors studied operate, in application relevant conditions, in a reaction limited regime as assumed in the paper. For square resonators of dimensions varying between 10 µm and 200 µm, with a microfluidic channel transporting the analytes to the surface with pressure up to 100 p.s.i. (limited by mechanical failure of the devices) and typical diffusion coefficients of the analytes ($4.1 < D(\cdot 10^7)[cm^2/s] < 12.9$, see [1]), the dimensionless Peclet numbers for the channel and the sensor (Pe_h and Pe_s respectively [2]) are larger than one (i.e. $Pe_h >> 1$ and $Pe_s >> 1$). In this case, the flux J is given by: $J \approx 0.81 Pe_s^{1/3} + 0.71 Pe_s^{-1/6} - 0.2 Pe_s^{-1/3}$. Since, in the same conditions, $Da << 1$ we are operating in a reaction limited regime [2]. Da is the Damkohler number given by $Da = k_{on} b_m A_s/(J/c_o)$, where k_{on} is the rate of association, c_o is the concentration, A_s is the surface area of the sensor and b_m is the capture sites density. Please note that for the manuscript, we have taken $b_m = 6.5 \times 10^{11}$ /cm^2. This was assumed to represent an average binding density of antibody immobilised on a surface based on the work by Zhang *et al.* [3].

MONTE CARLO SIMULATION: DETAILS AND EVALUATION

The Monte Carlo model was written using *Sage 6.2* (an open-source mathematical software using a Python based language). The following abbreviations are used in this section: Square$_{lame}$ and Square$_{SE}$ for square resonators excited in Lamé or square extension mode respectively, Beam$_{ext.}$ for beams in extensional mode and Beam$_{flex.}$ for cantilevers in dynamic mode. Table (I) shows, for each sensor studied, the standard deviation for a number of objects randomly positioned on the sensor. The values match well with the expression for the stochastic LOD (equation 2 in the manuscript). Fig.(3) shows the normal distributions for all the sensors for 200 molecules and a population of 500 measurements. The pseudo-random numbers in *Sage* were generated using the default seed that comes from os.urandom(), an operating system specific, truly random number. The results did not change by choosing arbitrary seeds as shown in Table (II). We have also verified the validity of the model by confirming that the results (standard deviation) are independent from the mass to be weighed, the effective mass and the dimensions of the sensors (data not shown).

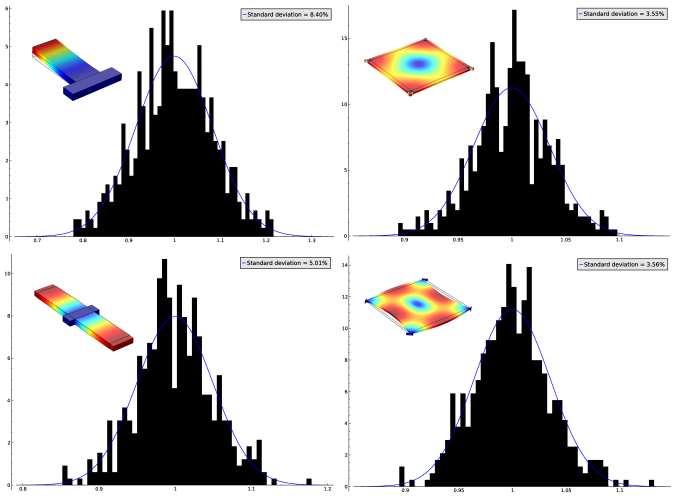

FIG. 3: Normal distribution of the normalised response for each resonator studied. The measurements are for 200 objects and a sample size of 500 measurements.

n	10	50	100	600
Square_{lame}	15.6%	7.17%	5.05%	2.08%
Square_{SE}	15.8%	6.91%	5.05%	2.06%
$\text{Beam}_{ext.}$	22.1%	9.78%	7.10%	2.81%
$\text{Beam}_{flex.}$	37.0%	16.6%	11.6%	4.76%

TABLE I: Standard deviation (σ) for a number of objects for each sensor topology considered. The results are for a population of 5000 measurements.

seed	default	0	1	24573
Square_{lame}	3.56%	3.54%	3.58%	3.52%
Square_{SE}	3.56%	3.55%	3.51%	3.54%
$\text{Beam}_{ext.}$	4.94%	5.05%	4.97%	5.08%
$\text{Beam}_{flex.}$	8.28%	8.12%	8.24%	8.40%

TABLE II: Standard deviation for each sensor comparing the default random number with arbitrarily chosen seeds. The results are for 200 objects and a population of 500 measurements.

[1] Garca De La Torre, J., Huertas, M. L. & Carrasco, B. Calculation of hydrodynamic properties of globular proteins from their atomic-level structure. *Biophys. J.* **78,** 719730 (2000).

[2] Squires, T. M., Messinger, R. J. & Manalis, S. R. Making it stick: convection, reaction and diffusion in surface-based biosensors. *Nat. biotech.* **26,** 417-426 (2008).

[3] Zhang, S., Garcia-D'Angeli, A., Brennan, J. P. & Huo, Q. Predicting detection limits of enzyme-linked immunosorbent assay (ELISA) and bioanalytical techniques in general. *Analyst* **139,** 439-445 (2014).